ACOUSTOFLUIDIC BEHAVIORS OF ZNO/AL PLATE/SHEET ACOUSTIC WAVE DEVICES USING HYBRID MODES

Yong Wang[1,2,3], Qian Zhang[3], Ran Tao[4], Dongsheng Li[3], Yongqing Fu[4,], and Jin Xie[3,*]*

[1] Key Laboratory of 3D Micro/Nano Fabrication and Characterization of Zhejiang Province, School of Engineering, Westlake University, Hangzhou 310024, China

[2] Institute of Advanced Technology, Westlake Institute for Advanced Study, Hangzhou 310024, China

[3] State Key Laboratory of Fluid Power and Mechatronic Systems, Zhejiang University, Hangzhou 310027, China

[4] Faculty of Engineering and Environment, University of Northumbria, Newcastle upon Tyne NE1 8ST, UK

ABSTRACT

In this paper, we report acoustofluidic behaviors of zinc oxide (ZnO) thin film surface acoustic wave (SAW) devices fabricated on aluminum (Al) plate/sheet (600μm/200μm) substrates using hybrid modes. Finite element analysis (FEA) simulation and experimental results indicate that the wave vibration modes are changed from Rayleigh mode to hybrid modes and subsequently to Lamb wave modes with the increased device's wavelength or decreased substrate thickness. For the Rayleigh, hybrid and zero-order Lamb wave modes, the droplet movement is a combination of rolling and sliding, whereas for Sezawa mode and one-order Lamb wave modes, the droplet movement is a combination of jumping and sliding. Moreover, for Lamb wave modes, the asymmetrical modes present a better pumping performance than those of symmetrical modes.

KEYWORDS

Acoustofluidics, ZnO thin film, Al plate/sheet, SAW, hybrid modes

INTRODUCTION

Applications of surface acoustic waves (SAWs) in microfluidic platforms (often called acoustofluidics) have attracted great interest for actuation and manipulation of fluids, microparticles/cells, in either a digital format (sessile droplet) or continuous flow (fluids inside a microchannel/chamber) [1-3]. They have shown superior advantages over other methods, such as simple structure design, small size, low cost, non-invasive and contact-free manner and high precision [4,5]. Conventional SAW devices for acoustofluidics are mostly made on bulk $LiNbO_3$ substrates due to their large piezoelectric constant and high electromechanical coupling coefficients (5~11%) [6]. However, these bulk substrates are generally expensive, less easily integrated with electrics and easily broken at a high power [7]. In addition, it is difficult to realize multiple wave modes or apply complex electrode designs on these substrates due to their anisotropic piezoelectric properties.

In comparisons with bulk piezoelectric substrates, SAW technologies based on piezoelectric thin films, e.g., ZnO films, present several distinct advantages, in terms of device design flexibility, cost and easiness of fabrication and integration with other electrics [8]. Moreover, as piezoelectric thin films are easily deposited onto various substrates such as silicon, glass, polymer and metal, various acoustic velocities, wave vibration modes and some new functions are then achieved [9-12]. Therefore, SAW technologies based on piezoelectric thin films have also been regarded as one of the key future directions for acoustofluidics. In recent years, various essential microfluidic functions, including streaming, mixing, concentration, pumping, jetting and nebulization have been realized using thin film surface acoustic waves with Rayleigh (R_0) mode [5, 8, 10]. However, up to now, acoustofluidics behaviors using thin film SAWs based on hybrid modes or Lamb wave modes have not been systematically investigated.

In this paper, we fabricate the ZnO thin film SAW devices with different wavelengths (varying from 100 μm to 400 μm) on Al plate/sheet (600μm/200μm) substrates and analyzed the effects of device's wavelength and substrate thickness on wave vibration modes through FEA simulation and experimental verifications. Moreover, for the first time, we systematically investigate acoustofluidic behaviors of thin film SAWs under Sezawa mode, hybrid modes and Lamb wave modes.

NUMERICAL MODELING

To understand the wave vibration patterns on Al plate/sheet, finite element analysis using commercial COMSOL Multiphysics (5.4) software with solid mechanics and electrostatic modules was performed. A simplified two-dimensional (2D) model with ideal material parameters, one pair of the interdigital transducer (IDT) electrodes, and periodic boundary conditions were used to simulate the wave modes of the SAW devices with different wavelengths and substrate thicknesses. For the FEA simulation, the thickness of metal (Au) electrode was set as 100 nm, the thickness of ZnO films was set to be 5 μm, the thicknesses of Al substrates were set to be 200 μm and 600 μm, respectively. The device's wavelengths were varied from 100 μm to 400 μm. A polarization voltage of 1V was assigned to one of metal electrode, while the other was assigned to be ground. Since thin film surface acoustic waves were often operating in plate mode, the bottom boundary condition of the Al substrate was set to be free. The material parameters of the ZnO films and Al substrate were obtained from the literature [13].

DESIGN AND FABRICATION

ZnO films of ~5 μm thick were deposited onto commercial Al plate/sheet substrates (with thicknesses of 600 ± 10 μm and 200 ± 5 μm) using DC magnetron

sputtering processes. For the film deposition, a zinc target with a purity of 99.999% was used. ZnO thin films were deposited onto the Al plate/sheet substrates using an Ar/O_2 gas flow rate of 10/13 sccm, a DC target power of 400 W, and a chamber pressure of ~3 mTorr. The distance between the target and the sample holder was 70 mm, and the sample holder was rotated during the deposition process to improve the uniformity of ZnO films. The thickness of ZnO films was controlled by the deposition time at a rate of ~5.6 nm/min. SAW devices were fabricated on the ZnO/Al plate/sheet substrates by patterning Cr (20 nm)/Au (100 nm) film to form the IDT electrodes using conventional photolithography and lift-off processes. Each IDT of the SAW devices was composed of 60 pairs of fingers, an acoustic aperture of 5 mm, and the device's wavelengths were varied from 100 μm to 400 μm. The reflection spectra (S_{11}) of the SAW devices were measured using an RF network analyzer (Agilent E5061B).

EXPERIMENTAL

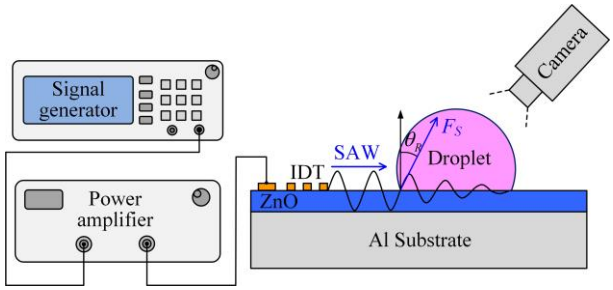

Figure 1: Schematic of experimental setup for microfluidic test.

Figure 1 shows the schematic of experimental up for microfluidic test. An RF input signal was generated using a signal generator (Marconi 2024, Plainview, USA) and amplified by a power amplifier (Amplifier research, 75A250, Souderton, USA). The amplified signal was then input into the IDT of the SAW device to drive the droplet. The input SAW power was measured using an RF power meter (Racal Instruments 9104). For microfluidic actuation tests, the surfaces of the SAW devices were treated with a layer of ~200 nm thick fluoropolymer coating (CYTOP, Asahi Glass Co., Tokyo, Japan) and heated to 120 °C for 10 min to make the surface hydrophobic. In addition, the SAW device was put onto an aluminum alloy test holder to increase the heat dissipation during the microfluidic test. The microfluidic behaviors for the SAW devices under different wave modes were observed using a standard video camera (60fps).

RESULTS AND DISCUSSION

In previous studies [13], we have shown that the ratio of wavelength to total substrate thickness (the combined thickness of ZnO/Al) plays an important role in wave mode generation. When this ration is much smaller than 1, Rayleigh wave mode are dominant. On the contrary, if the ratio is larger than 1, flexural types of Lamb waves are dominant, propagating through the whole substrate. When this ratio is nearly 1, the hybrid modes (both the Rayleigh mode and Lamb wave modes) are generally observed.

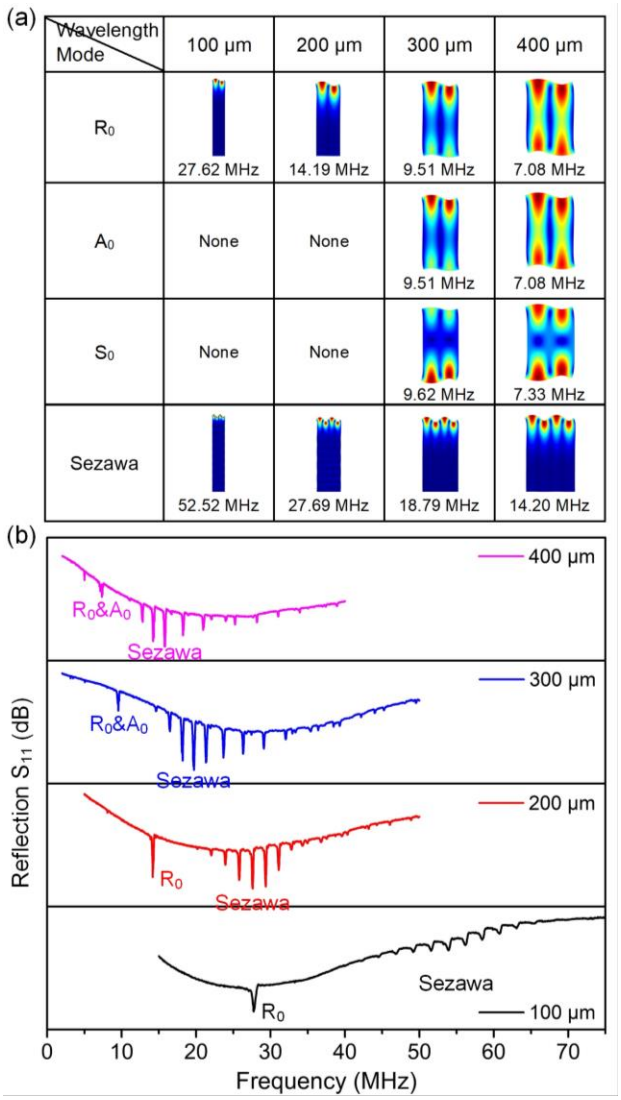

Figure 2: (a) FEA simulation of wave modes and (b) the measured reflection spectra for the SAW devices with wavelengths varying from 100 to 400 μm and Al substrate thickness of 600 μm.

Figure 2 shows FEA simulation of wave vibration modes and measured reflection spectra (S_{11}) for the SAW devices with the wavelengths varied from 100 to 400 μm and Al substrate thickness of 600 μm. It can be observed that Rayleigh mode and Sezawa mode appear in the devices with the wavelengths of 100 μm and 200 μm. However, for the SAW devices with the wavelengths of 300 μm and 400 μm, pseudo-Rayleigh mode and pseudo-A_0 mode of Lamb waves are hybridized together. Simultaneously at these two wavelengths, pseudo-S_0 mode of Lamb waves and Sezawa mode waves are also obtained. The results are in good agreements with the previous studies.

We further investigate the wave mode generation for the SAW devices with the wavelengths varying from 100 to 400 μm and reduced Al substrate thickness of 200 μm, with the results shown in Figure 3. The Lamb wave mode is clearly observed in the SAW devices with the wavelengths of 300 μm and 400 μm. The pseudo-A_1 mode and pseudo-Sezawa mode are hybridized together at a resonant frequency of 18.72 MHz for the SAW device with

wavelength of 300 μm. There is another hybridized mode of pseudo-R_0 and pseudo-A_0 at a frequency of 13.80 MHz in the SAW device with a wavelength of 200 μm. For the SAW device with the wavelength of 100 μm, there are only Rayleigh mode and Sezawa mode observed, without appearance of Lamb wave modes.

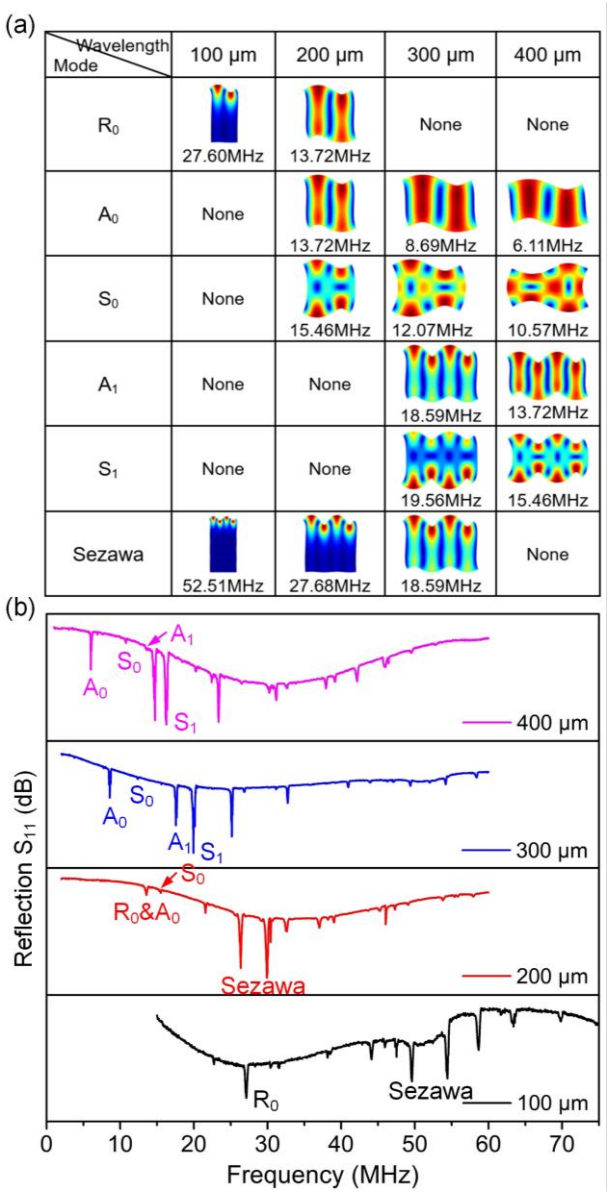

Figure 3: (a) FEA simulation of wave modes and (b) the measured reflection spectra for the SAW devices with wavelengths varying from 100 to 400 μm and Al substrate thickness of 200 μm.

Then we further investigate acoustofluidic behaviors of these SAW devices using different wave modes. Figure 4 shows droplet (1 μL) pumping images for the SAW devices with the wavelengths varied from 100 to 400 μm and Al substrate thickness of 600 μm using different wave modes. It can be observed that for the Rayleigh mode and zero-order pseudo-Lamb wave mode (pseudo-A_0 and pseudo-S_0), the droplet movement is a combination of rolling and sliding. However, for the Sezawa mode, the droplet movement is a combination of jumping and sliding, as shown in Figure 5.

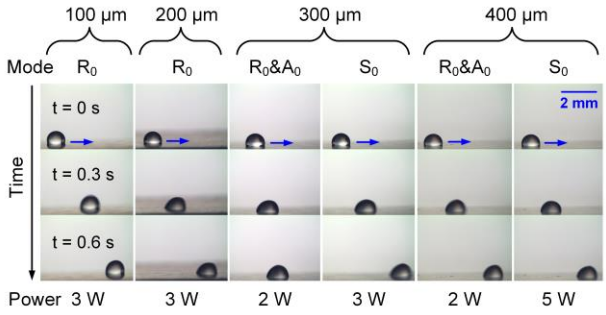

Figure 4: Droplet pumping images for ZnO/Al plate (600μm thick) SAW devices with different wavelengths using different wave modes.

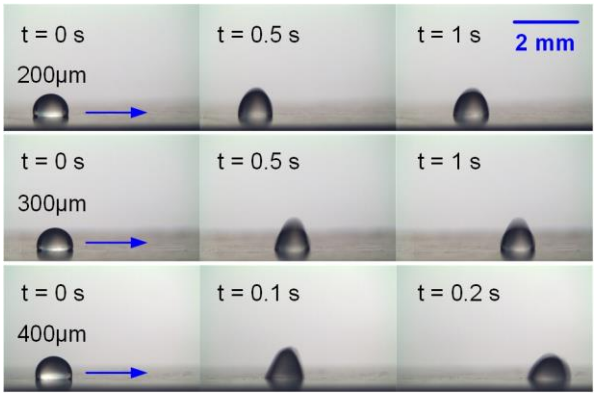

Figure 5: Droplet pumping images for ZnO/Al plate (600μm thick) SAW devices with wavelengths of 200 to 400 μm using sezawa mode.

According to the droplet motion video, the pumping velocities can be estimated. Figure 6 shows the average pumping velocities of the droplet (1 μL) for ZnO/Al plate SAW devices with different wavelengths using different wave modes under different input powers. Clearly, as the input power is increased, the droplet pumping velocity is increased. In addition, the Rayleigh mode and pseudo-A_0 mode present a better pumping performance than those of pseudo-S_0 mode and Sezawa mode. Furthermore, as the wavelength increases, the Rayleigh mode or pseudo-A_0 mode present a higher pumping velocity.

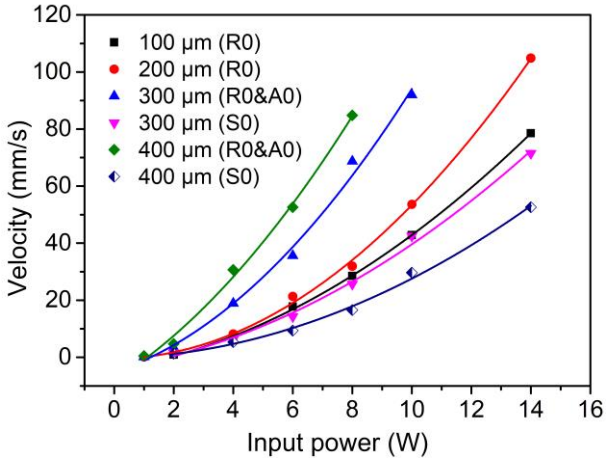

Figure 6: Droplet average pumping velocities for ZnO/Al plate (600μm thick) SAW devices using different wave modes under different input powers.

Figure 7 shows droplet (1 μL) pumping images for ZnO/Al sheet SAW devices with wavelengths of 100 μm, 200 μm and 400 μm using different wave modes. From which, we can see that for the Rayleigh mode and zero-order Lamb wave mode (A_0 and S_0), the droplet movement is a combination of rolling and sliding. Whereas, for one-order Lamb wave mode (A_1 and S_1), the droplet movement is dominated by the jumping and sliding.

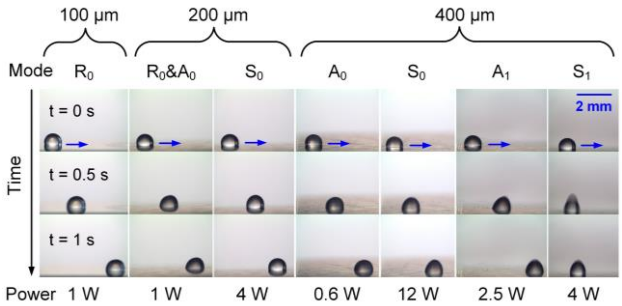

Figure 7: Droplet pumping images for ZnO/Al sheet (200 μm thick) SAW devices with the wavelengths of 100 μm, 200 μm and 400 μm using different wave modes.

CONCLUSIONS

Acoustofluidic behaviors of ZnO/Al plate/sheet acoustic wave devices using hybrid modes have been systematically investigated. Effects of device's wavelength and Al substrate thickness on wave generation modes are studied through both the FEA simulation and experiment verifications. Results show that as the device's wavelength increases or Al substrate thickness decreases, the wave mode will change from Rayleigh mode to hybrid modes and subsequently to Lamb wave modes. For the Rayleigh mode, hybrid modes and zero-order Lamb wave modes (A_0 and S_0), the droplet movement is a combination of rolling and sliding, whereas for Sezawa mode and one-order Lamb wave modes (A_1 and S_1), the droplet movement is dominated by jumping and sliding. Moreover, the Rayleigh mode and A_0 mode present a better pumping performance than those of S_0 mode and Sezawa mode.

ACKNOWLEDGEMENTS

This work is supported by the National Natural Science Foundation of China under Grant No. 51875521, the Zhejiang Provincial Natural Science Foundation of China under Grant No. LZ19E050002, the Engineering Physics and Science Research Council of UK (EPSRC EP/P018998/1) and UK Fluidic Network (EP/N032861/1) Special Interest Group of Acoustofluidics, International Exchange Grant (IEC/NSFC/201078) through the Royal Society, and the National NSFC.

REFERENCES

[1] S. Maramizonouz, X. Tao, M. Rahmati, et al., "Flexible and bendable acoustofluidics for particle and cell patterning," *Int. J. Mech. Sci.*, vol. 202, pp. 106536, 2021.

[2] Y. Q. Fu, J. K. Luo, N. T. Nguyen, et al., "Advances in piezoelectric thin films for acoustic biosensors, acoustofluidics and lab-on-chip applications," *Prog. Mater. Sci.*, vol. 89, pp. 31-91, 2017.

[3] P. Li, T. J. Huang, "Applications of acoustofluidics in bioanalytical chemistry," *Anal. Chem.*, vol. 91, no. 1, pp. 757-767, 2018.

[4] Y. Wang, Y. Wang, W. Liu, et al., "An aerosol sensor for PM1 concentration detection based on 3D printed virtual impactor and SAW sensor," *Sens. Actuators A: Phys.*, vol. 288, pp. 67-74, 2019.

[5] Y. Wang, X. Tao, R. Tao, et al., "Acoustofluidics along inclined surfaces based on AlN/Si Rayleigh surface acoustic waves," *Sens. Actuators A: Phys.*, vol. 306, pp. 111967, 2020.

[6] L. Y. Yeo, J. R. Friend, "Surface acoustic wave microfluidics," *Annu. Rev. Fluid Mech.*, vol. 46, pp. 379-406, 2014.

[7] Y. Wang, Q. Zhang, R. Tao, et al., "A rapid and controllable acoustothermal microheater using thin film surface acoustic waves," *Sens. Actuators A: Phys.*, vol. 318, pp. 112508, 2021.

[8] J. Zhou, H. F. Pang, L. Garcia-Gancedo, et al., "Discrete microfluidics based on aluminum nitride surface acoustic wave devices," *Microfluid. Nanofluid.*, vol. 18, no. 4, pp. 537-548, 2015.

[9] W. Wang, X. He, J. Zhou, et al., "Comparative study on microfluidic performance of ZnO surface acoustic wave devices on various substrates," *J. Electrochem. Soc.*, vol. 161, no. 10, pp. B230-236, 2014.

[10] Y. Wang, Q. Zhang, R. Tao, et al., "Flexible/bendable acoustofluidics based on thin-film surface acoustic waves on thin aluminum sheets," *ACS Appl. Mater. Interfaces*, vol. 13, no. 14, pp. 16978-16986, 2021.

[11] Q. Zhang, Y. Wang, T. Wang, et al., "Piezoelectric smart patch operated with machine-learning algorithms for effective detection and elimination of condensation," *ACS sensors*, vol. 6, no. 8, pp. 3072-3081, 2021.

[12] H. Jin, J. Zhou, X. He, et al., "Flexible surface acoustic wave resonators built on disposable plastic film for electronics and lab-on-a-chip applications," *Sci. Rep.*, vol. 3, no. 1, pp. 1-8, 2013.

[13] R. Tao, W. B. Wang, J. T. Luo, et al., "Thin film flexible/bendable acoustic wave devices: Evolution, hybridization and decoupling of multiple acoustic wave modes," *Surf. Coat. Technol.*, vol. 357, pp. 587-594, 2019.

CONTACT

*Jin Xie, tel: +86-571-87952274; xiejin@zju.edu.cn
*Richard Fu, E-mail: Richard.fu@northumbria.ac.uk